International Journal of Heat and Mass Transfer 52 (2009) 1421–1430

Contents lists available at ScienceDirect

International Journal of Heat and Mass Transfer

journal homepage: www.elsevier.com/locate/ijhmt

Efficiency of optimized bifurcating tree-like and parallel microchannel networks in the cooling of electronics

W. Escher [a,b], B. Michel [a], D. Poulikakos [b,*]

[a] IBM Research GmbH, Zurich Research Laboratory, 8803 Rüschlikon, Switzerland
[b] Laboratory of Thermodynamics in Emerging Technologies, Department of Mechanical and Process Engineering, ETH Zurich, 8092 Zurich, Switzerland

ARTICLE INFO

Article history:
Received 25 February 2008
Available online 17 October 2008

Keywords:
Bifurcating networks
Microchannel
Heat transfer
Fractals

ABSTRACT

A bifurcating tree-like network consists of a single inlet channel, which bifurcates over several levels to uniformly distributed microchannels that are vertically connected to a second network for fluid return. Here we introduce a one-dimensional model that considers convective heat transfer from the solid into the liquid as well as entrance and mixing effects. The performance of the bifurcating network is compared with that of a parallel microchannel cold plate branching from a single tapered manifold channel in terms of a constant volume flow rate, pressure gradient, and required pumping power. We optimized both networks independently with regard to global boundary conditions for cooling microprocessors and found a significantly superior performance for the parallel channel cooler. For a constant flow rate, the parallel channel network achieves a more than fivefold higher performance coefficient than the bifurcating tree-like network, while almost four times more heat can be removed for a constant pressure gradient across the networks.

1. Introduction

The past few decades have seen a rapid growth in the computational power of processor chips, which may continue as predicted by Moore's law. The exponential increase in transistor density and storage density as well as the faster clock speed, however, cause serious problems in the thermal management of microelectronic devices. This miniaturization trend renders thermal management challenging, especially when strict limitation of space and operating costs are applied. Until now the CPUs are cooled using large air heat sinks, but this will not be sufficient for cooling the next generation of microchips [1], particularly in compact multichip modules and 3-D microelectronic packages. Hence, novel cooling methods with thin form factors and high cooling performance are needed.

Tuckerman and Pease [2] first demonstrated microchannel heat sinks for cooling integrated electronic circuits. Since then, several investigations on single, straight microchannels and microchannel networks have been performed [3,4]. Microchannel heat sinks not only entail an increased heat transfer area per unit volume, they also make use of an enhanced solid to liquid heat transfer because of their narrow channel cross-section. However, the heat transfer enhancement is achieved at the expense of an increased pumping power. An additional disadvantage of parallel microchannel networks is the nonuniform wall temperature due to the fluid temperature increase along the channel. This has created a need for alternative designs.

Thanks to the evolution principle of survival of the fittest, nature often demonstrates optimal solutions for information handling and fluid transport problems. Because of the analogy between heat and mass transfer, biological transport systems provided inspiration for the design of tree-like structured microchannel networks as high-performance heat sinks [5–11].

Bejan and Errera [5] introduced "constructal" microchannel networks as heat sinks for electronic devices. They studied the cooling performance of rectangular and disk-shaped hierarchical structured networks, and proposed designs for fluid flow with minimum flow resistance between a volume and a point.

Chen and Cheng [6] and Pence [7] analyzed a rectangular design of a fractal bifurcating channel net for cooling electronic chips and compared its performance with that of a parallel channel net. They adapted the specific geometrical and operation parameters of the parallel channel net to the fractal network. Chen and Cheng [6] assumed the flow to be laminar and fully developed, and neglected the pressure drop across bifurcations. The hydraulic diameter was identical to that of the initial channel of the fractal network. The length of the parallel channels was twice that of the initial channel of the fractal network, and the number of channels matched the total heat transfer area of the fractal network. The flow in each channel of the parallel channel net had the same velocity as in the initial channel of the fractal net. Over the entire range of investigation, the fractal network increased the heat transfer rate while reducing the pumping power. In contrast to

* Corresponding author. Tel.: +41 44 632 2738; fax: +41 44 632 1176.
E-mail address: dimos.poulikakos@ethz.ch (D. Poulikakos).

0017-9310/$ - see front matter © 2009 Published by Elsevier Ltd.
doi:10.1016/j.ijheatmasstransfer.2008.07.048

Nomenclature

A	surface area [m^2]
B	branching factor [−]
C	friction coefficient [−]
COP	coefficient of performance [−]
c_p	specific heat capacity, 4198 [$J\,kg^{-1}\,K^{-1}$]
d	diameter [m]
f	Fanning friction factor [−]
h	channel height [m]
L	length [m]
N	quantity indicator [−]
Nu	Nusselt number [−]
P	pumping power [W]
p	pressure [Pa]
q''	area-normalized heat flux [$W\,cm^{-2}$]
R	frictional flow resistance [−]
Re	Reynolds number [−]
T	temperature [K]
u	velocity [$m\,s^{-1}$]
$\dot{V}$	volume flux [$m^3\,s^{-1}$]
w	channel width [m]
z	dimensionless channel length [−]

Greek letters

α	heat transfer coefficient [$W\,m^{-2}$]
β	Euclidean fractal dimension of diameter [−]
γ	Euclidean fractal dimension of length [−]
ε	aspect ratio, <1 [−]
ς	head loss coefficient [−]
λ	thermal conductivity, 0.599 [$W\,m^{-1}\,K^{-1}$]
μ	dynamic viscosity, 0.00102 [$kg\,m^{-1}\,s^{-1}$]
ξ	axial channel position [m]
ρ	density, 997.6 [$kg\,m^{-3}$]
0	zeroth branching level [−]

Subscript/Superscript

i,j	indices
k	branching level, index from 0 to K
K	total number of branching levels
M	manifold
x	x-direction
y	y-direction
chip	chip back-side surface, heat sink footprint
Ch	parallel channels
f	fluid
h	hydraulic
w	channel wall, convective surface
app	apparent
T	bifurcation
frict	frictional
p	parallel channel network
$\updownarrow$	mean

Chen and Cheng [6], Pence [7] took into account that the hydrodynamic and thermal boundary layers reinitiate after each bifurcation in the branching flow network. The parallel channels have a square cross-section, assuming that the hydraulic diameter of the parallel channels was equal to the terminal hydraulic diameter of the fractal channel network. The convective surface areas of both configurations were identical. Pence demonstrated that under constant pumping conditions the fractal network yields a 60% lower pressure drop for the same flow rate and a 30 °C lower wall temperature than the parallel channel net.

In the present work, we analyze the hydrodynamic and thermal performance of a bifurcating network, evaluate its potential as a cooling system for high-power electronics, and compare it with a parallel microchannel cold plate. In contrast to former comparisons [6,7], both networks are optimized independently with regard to common global boundary conditions for electronic cooling solutions. As global constraints we take a given footprint of the heat sink, a single inlet and outlet channel, and an overall maximum pressure drop. The present one-dimensional model accounts for simultaneously developing flow and pressure losses across bifurcations. We discuss the hydrodynamic performance of both networks based on the pressure drop for a given volume flux, and identify the required pumping power. The thermal performance of the network is evaluated for a constant wall heat flux and a constant wall temperature boundary condition. We determine the characteristic coefficients of performance, and compare the network performance for constant volume flux, pressure gradient, and pumping power.

2. Network design

The flow enters a bifurcating tree-like network for convective cooling through an initial channel at the 0th branching level, and bifurcates successively to smaller and smaller channels until it reaches the smallest capillaries as shown in Fig. 1. As the fluid is now distributed over the entire chip surface, a second tree-like network, located on top of the first network, is required to serve as fluid collector. The two identical networks are vertically connected at the ends of the highest branching levels. The flow enters the collector network by vertical interconnects, and merges again successively into larger channels until it leaves the network through a single outlet, located directly on top of or opposite to the inlet. Hence, a closed fluid loop with integrated manifold is formed, and no additional lateral manifold is needed.

The design of a fractal bifurcating network is determined by just a few parameters, as the ratio of the channel length and characteristic diameter from one to the next branching levels are constant. The channel length ratio is defined as

$$\frac{L_{k+1}}{L_k} = B^{-1/\gamma}, \tag{1}$$

and the ratio of the characteristic channel diameter is given by

$$\frac{d_{k+1}}{d_k} = B^{-1/\beta}, \tag{2}$$

where B is the branching factor, which equals 2 for a bifurcating network; γ and β are the Euclidean fractal dimension of length and diameter, respectively. The symbols d_k and L_k indicate the characteristic diameter and length of a channel at branching level k, where k is an index running from zero to K.

For manufacturability, the channel geometry is restricted to a rectangular cross-sectional flow geometry with a constant height h. The characteristic diameter d in Eq. (2) (the hydraulic diameter) is replaced by the square root of the cross-sectional area as suggested by Muzychka and Yovanovich [12]. Hence

$$d_{\mathrm{h},k} = (hw_k)^{0.5}, \tag{3}$$

where w_k is the channel width at the kth branching level. Combining Eqs. (2) and (3) provides an explicit characterization for the $k+1$-level channel width, w_{k+1},

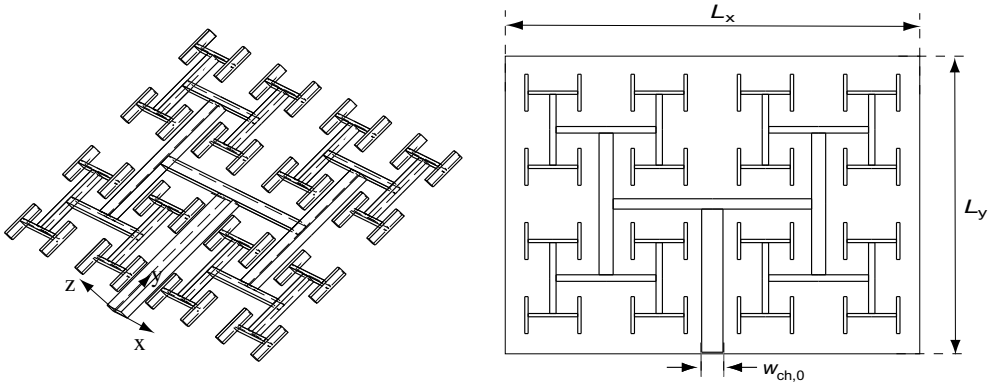

Isometric view Top view

Fig. 1. Bifurcating network with six branching levels $K = 6$, $d_{k+1}/d_k = 2^{-1/3}$, $L_{k+1}/L_k = 2^{-1/2}$ $L_0 = 10$ mm, $d_0 = 0.5$ mm.

$$w_{k+1} = w_k B^{-2/\beta}, \tag{4}$$

in terms of the lower branching level width, w_k. As the focus of this work is to design a heat sink for cooling a rectangular-shaped electronic chip, the branching angle is kept constant to 90°. According to Murray's law minimizing the network flow resistance for a fixed total channel volume leads to an optimal Euclidian fractal dimension for the length and width of $\gamma = 3$ and $\beta = 3$ [13]. However a Euclidian length scale factor of $\gamma = 3$ results in overlapping channels at higher branching levels. Thus, for geometric reasons, a factor of $\gamma = 2$ is chosen. Hence, for a given initial channel length L_0, channel width w_0 and channel height h, the only design parameter of freedom is the absolute number of branching levels.

Fig. 2 shows a scheme of a parallel channel network with an integrated manifold system. Fluid enters the network by a single manifold channel of initial width w_M. The manifold channel branches perpendicularly to narrow microchannels forming the heat-exchanging parallel channel network. The hot fluid is returned by a collecting channel with an outlet opposite to the inlet.

The parallel channel network covers exactly the same chip surface area as the tree-like network with uniformly distributed channels. Thus the dimensions of the surface in the x- and y-direction are given by

$$L_x = 4L_0 B^{-1/\gamma} \tag{5}$$

and

$$L_y = 2L_0. \tag{6}$$

As the fractal dimension of the channel length is 2, the footprint of the heat sink is determined by

$$A_{chip} = L_y L_x = 2^{5/2} L_0^2. \tag{7}$$

The maximum number of parallel channels is defined by the heat sink extension in the x-direction, the channel width, w_{Ch}, and the wall thickness, w_w, as

$$N_{Ch} \leqslant \frac{L_x}{w_{Ch} + w_w}, \tag{8}$$

where the number of channels, N_{Ch}, is an integer and is rounded down. The heat conduction in the solid part of the network is not taken into account. However, for a realistic design of a parallel channel network, a sufficiently high fin efficiency has to be ensured. Following Tuckerman and Peace [14], an optimum choice of design variables that minimize the overall thermal resistance is obtained by a channel width to wall thickness ratio of unity. The length of the parallel channels is determined from the extension of the heat transfer surface area in the y-direction and the initial width of the manifold $w_{M,0}$ to be

$$L_{Ch} = L_y - 2w_{M,0}, \tag{9}$$

and the length of the manifold channel is given by

$$L_M = L_x - 0.5w_w. \tag{10}$$

Each heat-exchanging microchannel is supplied by the same amount of fluid for the network to uniformly cool the surface area. Consequently the volume flux along the manifold channel decreases linearly with the axial position as

$$\dot{V}_M(\xi) = \left(1 - \frac{\xi}{L_M}\right), \tag{11}$$

where ξ is the channel axial position. To uniformly supply all heat-exchanging microchannels with fluid, a constant pressure drop across each microchannel is required. This will be established if the pressure along the supply and return channels drops linearly

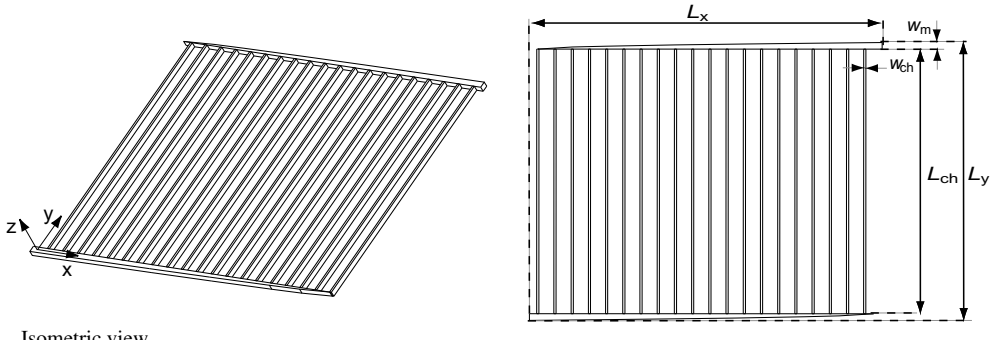

Isometric view Top view

Fig. 2. Parallel channel network with 20 parallel straight channels $N_{Ch} = 20$, $L_x = 28.33$ mm, and $L_y = 20$ mm.

with the same gradient. A nonlinearity of the pressure drop can be compensated by introducing a tapered channel cross-section. Assuming a laminar, fully developed flow, and a constant friction factor, we obtain a channel profile along the manifold:

$$w_{\mathrm{M}}(\xi) = w_{\mathrm{M},0}\left(1 - \frac{\xi}{L_{\mathrm{M}}}\right)^{1/2}. \tag{12}$$

This channel profile ensures that the pressure drop along the distribution and the collector manifold is the same, resulting in a constant pressure drop across all channels of the heat transfer network. Thus the channel width of the parallel network is the only independent parameter that provides freedom for optimizing the parallel channel network in terms of cooling power and efficiency.

3. Mathematical model

A mathematical model for computing the pressure distribution and heat transfer rates of both configurations was developed, assuming laminar and incompressible fluid flow with constant heat capacity, c_{p}, dynamic viscosity, μ_{f}, density, ρ_{f}, and thermal conductivity, λ_{f}. Senn and Poulikakos [11] demonstrated numerically that, when the flow passes a bifurcation, secondary flow motion occurs, causing laminar mixing of the fluid. Hence, both the hydrodynamic and thermal boundary layers are disrupted, and the pressure drop and heat transfer are increased locally. They demonstrated that the effect of bifurcations and turns is substantial and not negligible, if the hydrodynamic and the thermal boundary layers are assumed to reinitiate at the entrance of each branching level.

3.1. Hydrodynamic model

The pressure drop across a straight channel is found, assuming atmospheric pressure at the exit, by

$$\frac{\partial \bar{p}_{\mathrm{frict}}}{\partial \xi} = -\frac{2 f_{\mathrm{app}} \rho_{\mathrm{f}} \bar{u}^2}{d_{\mathrm{h}}}, \tag{13}$$

where f_{app} is the apparent Fanning friction factor. Muzychka and Yovanovich [15] developed a general model for hydrodynamically developing laminar flow in non-circular ducts by combining the asymptotic solutions of laminar boundary layer flow, Graetz flow, and fully developed flow for several duct configurations. The composite solution takes the form

$$f_{\mathrm{app},k} Re_k = \left[\left(\frac{12}{\sqrt{\varepsilon_k}(1+\varepsilon_k)\left[1 - \frac{192\varepsilon_k}{\pi^5}\tanh\left(\frac{\pi}{2\varepsilon_k}\right)\right]}\right)^2 + \left(\frac{3.44}{\sqrt{z_k^+}}\right)^2\right]^{1/2}, \tag{14}$$

where ε is the aspect ratio of the channel. The Reynolds number Re_k at the kth branching level is given by

$$Re_k \equiv \frac{\rho_{\mathrm{f}} \bar{u}_k d_{\mathrm{h},k}}{\mu_{\mathrm{f}}} \tag{15}$$

with the mean velocity $\bar{u}_k$ at the kth branching level

$$\bar{u}_k = \frac{\dot{V}_k}{d_{\mathrm{h},k}^2} = 2^{k(2/\beta-1)}\frac{\dot{V}_0}{h w_0}. \tag{16}$$

As a result, the frictional pressure drop across the kth branching level is given by

$$\Delta p_{k,\mathrm{frict}} = \frac{2 f_{\mathrm{app},k} \rho_{\mathrm{f}} \bar{u}_k^2 \xi_k}{d_{\mathrm{h},k}}. \tag{17}$$

The pressure drop across a bifurcation between the kth and the $k+1$th branching level is correlated with the dynamic pressure at the kth branching level, and is given by

$$\Delta p_{k,\mathrm{T}} = \zeta_{\mathrm{T}} \frac{1}{2}\rho_{\mathrm{f}} \bar{u}_k^2, \tag{18}$$

where the heat-loss coefficient is empirically determined to be $\zeta_{\mathrm{T}} = 1.3$ for a T-junction [16]. Consequently the overall pressure drop of the bifurcating network is identified as

$$\Delta p = 2\sum_{k=0}^{K}(\Delta p_{k,\mathrm{frict}} + \Delta p_{k,\mathrm{T}}), \tag{19}$$

where the factor 2 indicates that for simplicity the pressure drop in the second network is assumed to be identical to that of the first network, which imposes an identical heat loss for the bifurcating and the merging flow.

The overall pressure drop across a parallel network is determined by the frictional pressure drop across the manifold and the heat-exchanging straight channel,

$$\Delta p_{\mathrm{p}} = \Delta p_{\mathrm{M}} + \Delta p_{\mathrm{Ch}}. \tag{20}$$

Along the manifold channel, the volume flux decreases and the channel cross-section tapers according to Eqs. (11) and (12), respectively. Because the system has a finite number of channels branching from the supply system, the volume flux does not decrease linearly but discretely along the channel as

$$\dot{V}_n = \dot{V}_n\left(1 - \frac{n}{N_{\mathrm{Ch}}}\right), \quad \text{for } 0 \leqslant n \leqslant N_{\mathrm{Ch}}. \tag{21}$$

By integrating Eq. (13) along the manifold channel, the pressure drop across the supply system is given by Fig. 3

$$\Delta \bar{p}_{\mathrm{M,frict}} = \int_0^{L_{\mathrm{M}}} -\frac{2 f_{\mathrm{app}}(\xi,\bar{u})\rho_{\mathrm{f}}\bar{u}^2(\xi)}{d_{\mathrm{h}}(\xi)}\mathrm{d}\xi. \tag{22}$$

The integral is solved numerically by dividing the manifold channel into N_{Ch} segments that are discretized into N_{I} discrete volumes with a grid spacing Δx and a constant channel width as shown in Fig. 4. The pressure drop of each segment is calculated by summing up the pressure drop across each discrete volume. The pressure drop across a discrete volume is determined by

$$\Delta p_i^n = \Delta p(\xi^{n-1} + i\Delta x) - \Delta p(\xi^{n-1} + (i-1)\Delta x), \tag{23}$$

where i is a local node identifier. Hence, the overall pressure drop across the manifold channel is determined by

$$\Delta p_{\mathrm{M}} = \sum_{n=1}^{N_{\mathrm{Ch}}}\sum_{i=1}^{N_{\mathrm{I}}}\left\{f_{\mathrm{app},i}^{n-1}[\xi^{n-1} + i\Delta x] - f_{\mathrm{app},i-1}^{n-1}[\xi^{n-1} + (i-1)\Delta x]\right\}\frac{2\rho u_i^{n-1}}{d_{\mathrm{h},i}^{n-1}}. \tag{24}$$

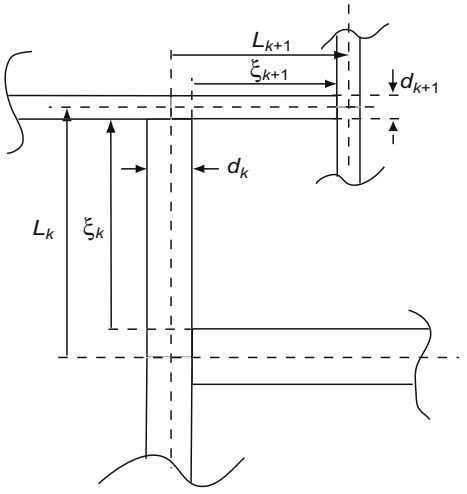

Fig. 3. Schematic of the geometrical structure of the bifurcating network.

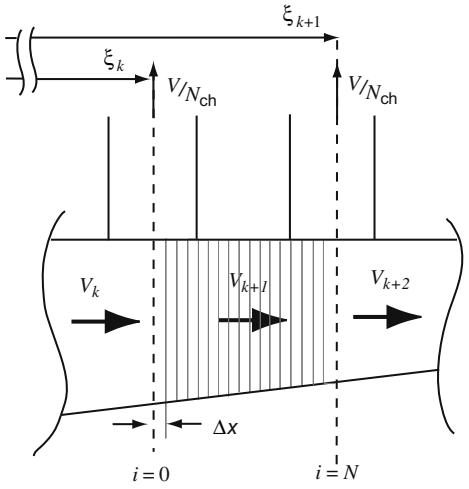

Fig. 4. Schematic of the geometrical structure and discretization scheme of the parallel channel network.

3.2. Thermal model

In the present model we do not explicitly consider heat conduction in the solid material between the fluid channels. Hence, we need to define a realistic boundary condition for the convective heat transfer from the channel wall into the liquid, which represents the heat flow from a chip back-side to the fluid channels. As in the bifurcating network the heat transfer coefficient changes from branching level to branching level, the heat flux from the chip back-side is conducted preferentially to the smaller channels at higher branching levels which have the highest heat transfer coefficient. A constant heat flux boundary condition does not apply. Typically the material being used to fabricate a heat sink is highly conductive. Assuming an infinite thermal conductivity of the heat sink material, there is no conductive thermal resistance, resulting in a constant channel wall temperature that is equal to the temperature of the chip back-side. In a real system with finite thermal conductivity, we find a boundary condition somewhere in between a constant wall temperature and a constant heat flux boundary condition. For the sake of simplicity, we apply the idealized boundary conditions of constant heat flux and constant temperature, and analyze the network performance for these two conditions.

The heat transfer from solid to liquid is computed numerically by means of a channel discretized into N_J segments. The heat flux from the solid wall into the liquid at branching level k and node j is computed using Newton's law of cooling,

$$q''_{k,j} = \alpha_{k,j}(T_{w,j} - T_{f,k,j}), \tag{25}$$

where α is the local heat transfer coefficient. As we consider the thermal boundary to reinitiate at each branching level, the heat transfer coefficient α is a function of position ξ_k and can be obtained by

$$\alpha(\xi_k) = \frac{Nu(\xi_k)\lambda_f}{d_{h,k}}, \tag{26}$$

where $Nu(\xi_k)$ is the local Nusselt number considering simultaneously developing flows. A correlation for a constant wall temperature and a constant wall heat flux boundary condition is provided by Muzychka and Yovanovich [17]. We determine the fluid temperature from an energy balance across a discrete volume ΔV as

$$T_{f,k,j} = T_{f,k,j-1} + \frac{q''_{k,j}A_{w,k,j}}{\rho\dot{V}_k c_p}, \tag{27}$$

where $A_{w,k,j}$ is the convective surface area of the discrete channel segment. To estimate the thermal performance of the heat sink we calculate the total removed heat normalized to the heat sink footprint

$$q''_{chip} = \rho\dot{V}_0 c_p \frac{A_w}{A_{chip}}(T_{f,K,N} - T_{in}). \tag{28}$$

For a constant wall heat flux boundary condition, we calculate the wall temperature along the channel network by solving Eq. (25) for $T_{w,i}$ with the local fluid temperature being determined by Eq. (27). We assume that the heat flux is introduced through the bottom surface of the heat sink and is distributed uniformly to all walls of the channel network, hence

$$q''_w = q''_{chip}\frac{A_{chip}}{A_w}. \tag{29}$$

4. Grid independence and validation

For the thermal model we reached convergence for $N_J = 2000$, and for the pressure drop along the manifold, cf. Eq. (24), for $N_l = 1400$. The present model of the bifurcating tree-like network is validated by numerical results from Senn and Poulikakos [11]. They numerically investigated laminar convective heat transfer and pressure drop characteristics in a bifurcating microchannel network by solving the three dimensional Navier–Stokes and energy equations for an incompressible fluid with constant properties. A constant heat flux is applied to the wall of the square cross-sectional channels with an inlet hydraulic diameter of 1 mm and an initial channel length of 10 mm. They considered two cases. In the first case, they applied a heat flux of 776.8 W/m^2 at a Reynolds number of 20, resulting in an overall pressure drop across the entire network of 4.88 Pa and a maximum wall temperature of about 352.5 K. In the second case, a heat flux of 7768 W/m^2 at a Reynolds number of 200 was applied. They computed a pressure drop of 64.3 Pa, and reached a maximum wall temperature of about 353 K. We adapted the geometry and the hydrodynamic and thermal boundary conditions of our model to their simulations. We found the pressure drops to be 3.9 and 58.3 Pa and maximum wall temperatures of 351.75 and 352.4 K at Reynolds numbers of 20 and 200, respectively, which is in good agreement with their results mentioned above.

5. Results and discussions

The hydrodynamic and the thermal model are numerically solved for a bifurcating and a parallel channel network with integrated manifold. The cross-section of the initial channel of both networks is square, with an initial channel width and height of 500 μm. The initial channel length of the bifurcating network is 10 mm, resulting in a rectangular surface area of 2×2.833 cm^2. The performance of both networks is evaluated in the laminar flow regime with Reynolds numbers of less than 2000 in the entrance of the initial channel. The inlet fluid temperature is 293 K, and we assume constant fluid properties, representing liquid water at the inlet temperature. In this section we discuss the influence of the volume flux and the geometric parameters of freedom, such as the number of branching levels for the bifurcating network and the channel width for the parallel network, on the performance of the corresponding network.

5.1. Tree-like network

Fig. 5a shows the frictional pressure drop and the pressure drop across a bifurcation at each branching level for bifurcating networks with different total numbers of branching levels. A constant pressure gradient of 30 kPa bar is applied across the entire network. The frictional pressure drop across the initial channel

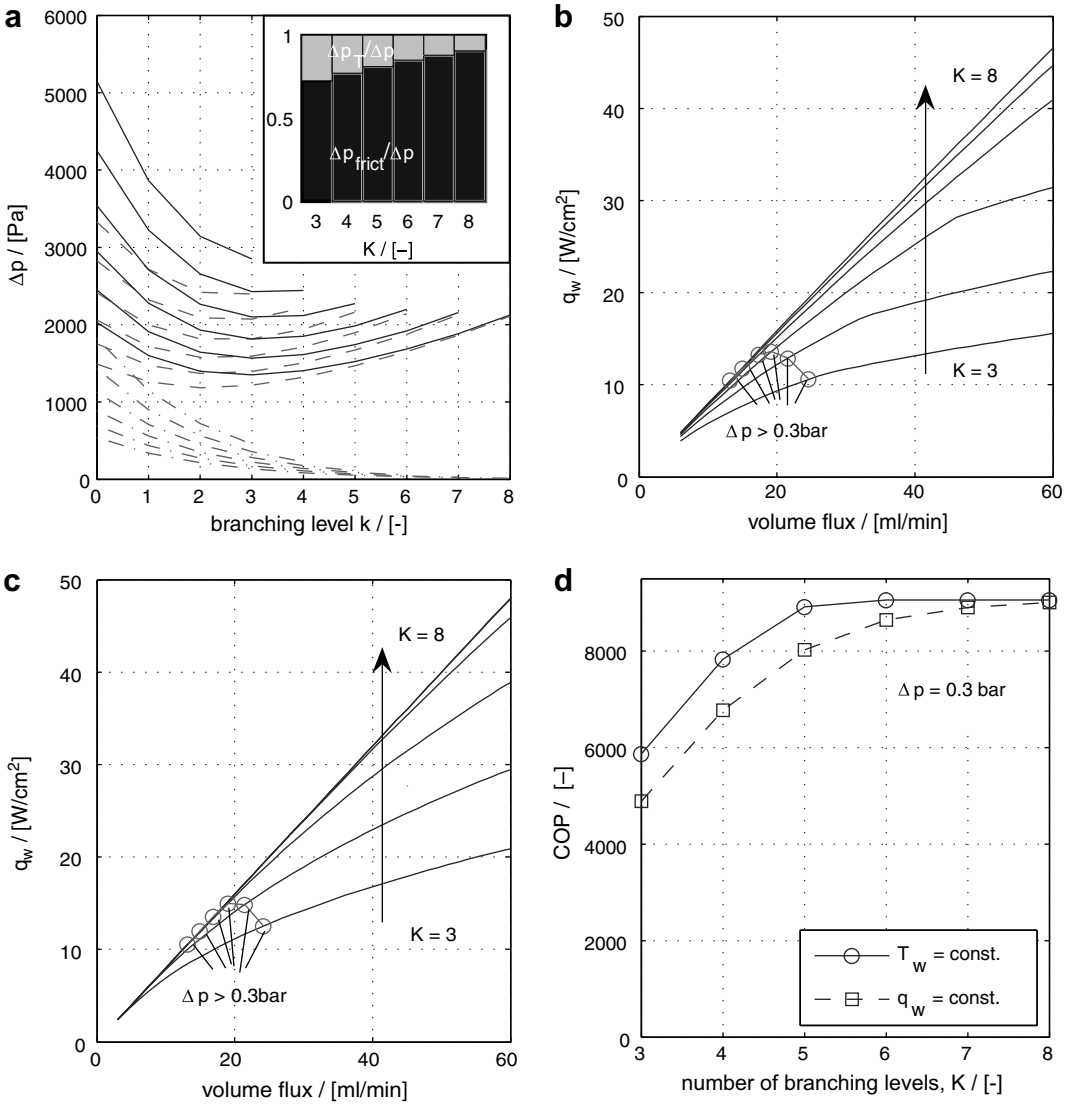

Fig. 5. (a) Pressure drop as a function of branching level for networks with different total numbers of branching levels; solid line: overall pressure drop across branching level, dashed line: frictional pressure drop, dashed-dotted line: pressure drop across bifurcation; (b) dissipated heat as a function of volume flux for networks with different total number of branching levels, constant wall heat flux boundary condition. Dots indicate a total pressure drop of 30 kPa across the entire network; (c) as (b) but for a constant wall temperature; (d) COP for networks with different total numbers of branching levels for constant wall heat flux and constant wall temperature boundary condition.

decreases with an increasing number of branching levels. If an additional branching level is added to the network, the total length of the flow path and hence also the flow resistance will increase. Consequently, for a constant pressure gradient, the total volume flux through the network diminishes and the frictional pressure loss across the initial channel drops. The pressure drop across a bifurcation decreases from one branching level to the next as the volume flux in a single channel is reduced. The bar plot in Fig. 5a shows the contribution of the pressure drop across bifurcations and of the frictional pressure drop to the overall pressure drop. The contribution of the pressure drop across bifurcations to the overall pressure drop of the network is significant. For networks with three branching levels, 27.6% of the overall pressure drop is caused by splitting the flow at bifurcations, whereas for the network with a total number of 8 branching levels it still contributes 9.8% to the overall pressure loss. Therefore, especially for networks with a higher total number of branching levels, the overall pressure drop is dominated by the frictional flow resistance. The pressure drop across bifurcations has only a minor influence on the change in network performance due to the adding of additional branching levels.

For a network with only three branching levels, the frictional pressure loss across each branching level decreases with increasing branching level, cf. Fig. 5a. The frictional flow resistance at one branching level is defined as

$$R_k = \frac{C_{\mathrm{app}} \dot{V}_k L_k}{d_{\mathrm{h},k}^4}, \tag{30}$$

where C_{app} is the apparent friction coefficient and is given by

$$C_{\mathrm{app},k} = \frac{f_{\mathrm{app},k}(L_k)}{Re_k}. \tag{31}$$

The volume flux in a single network channel decreases by a factor of two at each branching level. If the channels are of a square cross-section and the flow is fully developed, the friction coefficient will remain constant for all channels. Hence, with respect to Eqs. (1) and (2) the frictional flow resistance will decrease from branching level to branching level by a factor of $2^{-1/6}$. However, as in the present study the channel height is constant and only the channel width changes and as we also consider entrance effects, the friction coef-

ficient is a function of the channel aspect ratio and the channel entrance length, cf. Eq. (14). Thus it changes from branching level to branching level. If the apparent friction coefficient rises by more than a factor of $2^{1/6}$, the overall frictional flow resistance will increase from one to the next branching level, causing an increase of the frictional pressure drop at higher branching levels as seen in Fig. 5a.

The frictional pressure drop of networks with five and more branching levels increases from the 3rd branching level on, whereas for networks with fewer branching levels it decreases up to the 4th branching level. This is caused by entrance effects. The contribution of entrance effects is a function of the dimensionless channel length z^+. If z^+ increases, the influence of entrance effects will become weaker. The dimensionless channel length at the kth branching level is a function of the physical channel length, L_k, and the channel's Reynolds number, Re_k. Combining the channel's Reynolds number ratio $Re_{k+1}/Re_k = 2^{-2/3}$ with Eq. (1) yields the ratio for the dimensionless channel length: $z^+_{k+1}/z^+_k = 2^{1/2}$. Hence entrance effects become weaker at higher branching levels. This is observed for the network with just three branching levels, whose pressure drop is mainly dominated by entrance effects. As the overall volume flux decreases with a higher total number of branching levels, entrance effects become less significant. Consequently the pressure drop of networks with higher branching levels is dominated by the flow in the fully developed region described by the first term in Eq. (14).

For a constant pressure drop, the flow rate decreases with an increasing number of branching levels. On the other hand, both the heat transfer area and the solid to liquid heat transfer increase. Hence, there will be an overall optimum number of branching levels. We evaluate the thermal performance for a constant wall heat flux boundary condition and a constant wall temperature. For a constant wall heat flux boundary condition, we determined the tolerable wall heat flux that provides a maximum wall temperature of less than 358 K. In the case of a constant wall temperature boundary condition of 358 K, we investigated the dissipated heat. We computed the dissipated heat as a function of the total number of branching levels for a constant wall heat flux and a constant wall temperature boundary condition as shown in Fig. 5b and c, respectively. As expected, more heat is dissipated with increasing volume flux and with increasing total number of branching levels. Fig. 5b shows that for networks with a lower number of branching levels the slope of the curve changes and becomes flatter with increased volume flux. If the volume flux is increased, the thermal resistance due to the finite heat capacity of the fluid will drop, whereas the convective thermal resistance is a weak function of the volume flux. The convective heat transfer depends on the volume flux only in the entrance region of a channel. If the volume flux is increased the entrance length is elongated, and thus the solid to liquid heat transfer is enhanced because of the enhanced mixing of the fluid perpendicularly to the flow direction. However, in the thermal and hydrodynamic fully developed flow region of the channel, an increased volume flux does not influence the convective thermal resistance. Hence, at low volume fluxes, the heat transfer is limited by the finite heat capacity of the fluid and increases linearly with volume flux. At higher volume fluxes the contribution of the convective thermal resistance to the overall thermal resistance increases and hence reduces the thermal benefit of an increased volume flux. This trend is more pronounced for networks with a lower total number of branching levels. If the number of branching level is increased the convective thermal resistance decreases. Hence the region being dominated by the convective thermal resistance is shifted to higher volume fluxes.

In addition, we investigated the heat transfer for a constant wall temperature boundary condition to evaluate the influence of the boundary condition on the thermal performance of the network. As shown in Fig. 5c, the dependency between the dissipated heat and the volume flux is similar to that of the constant wall heat flux boundary condition. The absolute numbers of dissipated heat are slightly higher for a constant wall temperature because the fluid experiences a larger average temperature gradient while passing through the network.

The efficiency of a heat sink is determined by its coefficient of performance, COP. The coefficient of performance is defined as the ratio of the dissipated heat and the energy needed to remove the heat, and is given by

$$\mathrm{COP} = \frac{q''_{\mathrm{chip}} A_{\mathrm{chip}}}{P}, \tag{32}$$

where P is the required pumping power determined by the pressure drop across the network and the flow rate,

$$P = \Delta p \dot{V}. \tag{33}$$

For a practical implementation of a microchannel heat sink in an application, as for example a server rack, a pressure drop of about 30 kPa is desirable [18]. The dots in Fig. 5b and c indicate the volume flux and the dissipated heat for the limiting pressure drop. For a constant pressure drop boundary condition, the volume flux initially decreases with an increasing number of branching levels, whereas the overall convective heat transfer increases. The operation point of heat sinks with three and four branching levels is in the region governed by the solid to liquid heat transfer. For those networks, an additional branching level reduces the convective thermal resistance, whereas the thermal resistance due to the limited heat capacity of the fluid is increased only slightly because of a reduction of volume flux. Hence, in this region, the performance of the network is increased by increasing the number of branching levels, as seen in Fig. 5d. A maximum thermal performance is achieved if the heat sink is operated in the transition regime as for the network with $K = 5$. In this manner, we make use of the full heat capacity of the fluid at a minimum flow resistance. If more branching levels are added, the thermal performance is limited by the finite heat capacity of the fluid, and the dissipated heat decreases linearly with decreasing volume flux. For a constant pressure gradient, the dissipated heat and the required pumping power reduce likewise, and as a result the efficiency of the network is not significantly improved by further increasing the number of branching levels. As a network with a total number of branching levels of five exhibits the best thermal performance and because the efficiency does not change significantly for networks with higher branching levels, we select for the present boundary conditions an optimum number of branching levels of five.

5.2. Parallel channel network

The hydrodynamic and the thermal performance of a heat sink with parallel channels across the surface and an integrated manifold strongly depend on the width of the parallel heat exchange channels. The performance of the heat sink is analyzed in a Reynolds number range of 500–2000 in the entrance region of the manifold channel.

Fig. 6a shows the pressure drop across the manifold, the parallel microchannels, and the overall network as a function of the hydraulic diameter of the parallel mircochannels. As the hydraulic diameter decreases, the absolute number of channels increases, cf. Eq. (8), and hence the volume flux along the manifold channel and the volume flux in each heat-exchanging microchannel change. The reduction of volume flux along the manifold channel is compensated by the tapering of the channel cross-section. The pressure drop across the manifold channel is almost independent of the number of parallel channels, whereas the pressure-drop across the heat exchanging microchannels increases with decreasing

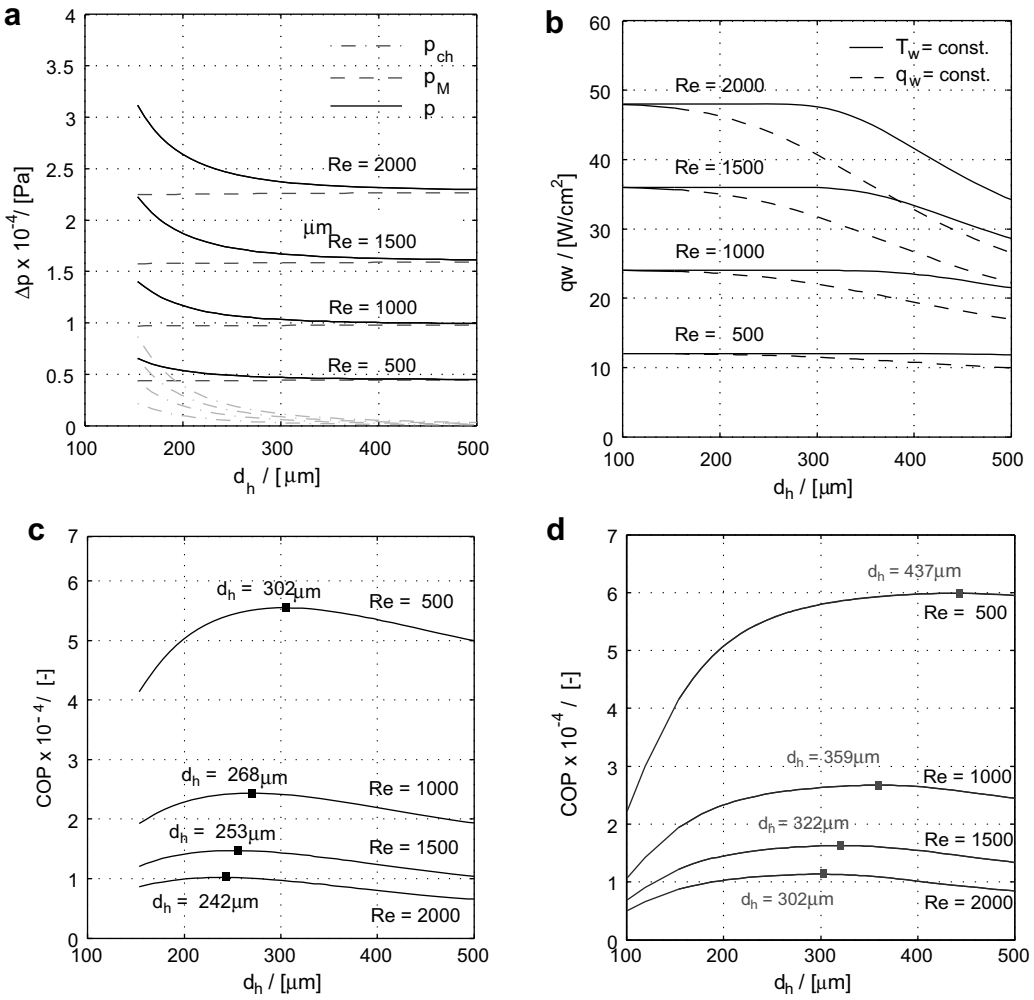

Fig. 6. (a) Pressure drop across the entire parallel channel network, across the manifold, and across the parallel straight channels as a function of hydraulic diameter; (b) dissipated heat as a function of hydraulic diameter for a constant wall heat flux and constant wall temperature boundary condition; (c) COP as a function of hydraulic diameter of the straight channels for a constant wall heat flux boundary condition; (d) COP as a function of hydraulic diameter of the straight channels for a constant wall temperature boundary condition.

hydraulic diameter. It follows from the superposition of both that the overall pressure drop increases with decreasing channel width.

As in the case of the bifurcating network, we evaluated the thermal performance of the network for a constant wall heat flux providing a maximum wall temperature of less than 358 K and for a constant wall temperature of 358 K. In both cases, the heat flux is normalized with respect to the footprint of the heat sink and is reported in Fig. 6b as a function of the hydraulic diameter of the parallel channels. For a constant wall heat flux, the maximum tolerable heat flux increases with decreasing hydraulic diameter because the solid to liquid heat transfer increases with decreasing channel cross-section, cf. Eq. (26). However, it can be seen from Fig. 6b that for channels with a small hydraulic diameter, the dissipated heat is not increased but is dominated by the thermal resistance because of the finite heat capacity of the fluid. The transition range separates the range being dominated by the finite heat capacity of the fluid from the range being dominated by the liquid to solid heat transfer. For a Reynolds number of 500, the dissipated heat is almost independent of the hydraulic diameter of the heat-transferring microchannels over the diameter range of interest. If the Reynolds number is increased, the transition range is more pronounced and is shifted to smaller diameters with increasing Reynolds numbers because the thermal resistance due to the finite heat capacity of the fluid decreases. A similar relationship between the dissipated heat and the hydraulic diameter is observed for a constant wall temperature boundary condition. The transition range is shifted to higher hydraulic diameters because for a constant wall temperature the average solid to fluid temperature gradient is larger than for a constant wall heat flux. Hence, the driving force for the solid to liquid heat transfer is increased and, as a result, the heat transfer is limited by the finite heat capacity of the fluid at smaller heat transfer coefficients than for the constant wall heat flux boundary condition.

To determine an optimum hydraulic diameter, we investigated the performance of the network dependence of the hydraulic diameter and the Reynolds number. There exists an optimum diameter as a function of Reynolds number, as seen from Fig. 6c. The optimum hydraulic diameter corresponds to the transition range observed for the heat transfer, cf. Fig. 6b. At the optimum hydraulic diameter, the full heat capacity of the fluid is used to remove heat at minimum pressure losses. For the heat transfer, the optimum hydraulic diameter is shifted to larger values for a constant wall temperature boundary condition, as seen from Fig. 6c and 6d. In all cases, the optima are quite flat, leaving some design freedom. In the following we will look at the conservative case of a constant wall heat flux boundary condition and take an optimum diameter of 242 μm.

5.3. Comparison: bifurcating vs. parallel channel network

In this section, we compare the performance of the parallel channel and the bifurcating network at their respective design optimum. We apply a constant wall heat flux boundary condition and determine the maximum tolerable heat flux that provides a wall temperature of less than 358 K. Table 1 shows a comparison of both networks for identical volume flux, pressure drop, and pumping power. For identical volume flux, both networks are operated in the range dominated by the thermal resistance because of the finite heat capacity of the fluid. Hence, as the volume flux and the fluid outlet temperature are the almost same, both networks dissipate roughly the same amount of heat. The pressure drop across the parallel channel network is 0.235 bar smaller than across the bifurcating network, resulting in an almost five times reduced pumping power and a 500% enhanced efficiency. For a constant pumping power, a volume flux of 39.93 ml/min flows through the parallel channel network. This is 20.1 ml/min higher than the flow rate for the bifurcating network, whereas the pressure drop across the parallel channel network is 0.152 bar lower than across the bifurcating network. The parallel channel network dissipates about twice the energy of the bifurcating network, resulting in a more than twofold increased overall efficiency. If the pressure drop across the networks is kept constant, 3.8 times more heat is dissipated by the parallel channel network than by the bifurcating network because of the more than three times higher volume flux, while the network efficiencies are almost identical.

The fractal structure and the limitation to a branching factor of two restrict the parameter of freedom of the bifurcating network drastically. The freedom to optimize the parallel channel network with respect to its branching factor affects the network to distribute fluid more efficiently to a larger surface area more than it does the bifurcating network. In the case of optimized networks, the parallel channel network distributes the fluid from a single inlet channel directly to 121 parallel microchannels, providing a heat transfer surface area of 28 cm^2 compared with a total surface area of the tree-like network of just 2.1 cm^2.

Earlier comparisons between bifurcating tree-like and parallel channel networks did not consider a manifold system for the parallel channel network. They only considered the hydrodynamic and thermal performance of the straight parallel channel network. If the pressure drop across the manifold is not taken into account, cf. Fig. 6, the parallel channel network will outperform the bifurcating network by an even much larger factor. Chen and Cheng [6] postulated an identical surface area of the networks and reported an enhanced efficiency of the bifurcating microchannel net. We demonstrated that a restriction in surface area is not an appropriate boundary condition for an efficiency comparison of different heat sink designs in realistic applications in electronics. Instead global boundary conditions, such as available space, form factor and constraints in operation parameters, will determine the optimal heat sink design.

Table 1
Comparison of flow rate, pressure drop, pumping power, dissipated heat, and coefficient of performance of a bifurcating network with five branching levels and a parallel channel network with 121 channels and a hydraulic diameter of 242 μm for different operation parameters and a constant wall heat flux boundary condition

Bifurcating network $K = 5$		Parallel channel network, $d_h = 242$ μm		
		$\dot{V}$ = constant	$p\dot{V}$ = constant	Δp = constant
$\dot{V}$ [ml/min]	19.2	19.2	39.3	69.1
Δp [bar]	0.3	0.065	0.148	0.3
$p\dot{V}$ [mW]	9.7	2.1	9.7	34.6
q [W cm^{-2}]	13.6	14.98	29.88	50.67
COP [−]	7933	40770	17387	8445

6. Conclusions

We presented a one-dimensional model to analyze the hydrodynamic and the thermal performance of a bifurcating and a parallel channel network branching from a single manifold channel. In contrast to earlier comparisons [6,7], both networks were optimized independently with respect to global boundary conditions, such as a thin form factor and a single fluid inlet and outlet. Because of the massive branching from the manifold, the parallel channel cooler is much more densely packed than the bifurcating network and distributes the coolant more efficiently to a larger heat transfer surface area. For a constant flow rate, the parallel channel network has a more than fivefold higher coefficient of performance than the bifurcating tree-like network, while almost four times more heat can be removed for a constant pressure gradient across the networks. In addition, the manifold system and the heat exchanging channels of the parallel channel network are integrated into a single plane, whereas the bifurcating design requires a second plane for fluid return. Consequently, the parallel channel design is less complicated in terms of manufacturing and requires only half the overall network height of the bifurcating network.

The drawback of the present parallel channel design is the nonuniformity in cooling capacity owing to the heating up of the fluid in the axial direction along the channels. The uniformity and the cooling capability can be improved by distributing the fluid more effectively over the surface to shorter heat-exchanging channels. To supply shorter channels distributed over the same surface area of the heat-generating device, either direct access from the top or, if only lateral access is feasible, a planar hierarchical manifold system is required. Bejan and Errera [19] proposed a concept for cooling a heat-generating volume by using networks with massive branching at the highest branching level and a hierarchical supply and return system with a heterogeneous branching factor. The parallel channel network branching from a single manifold channel investigated here can be thought of as a limit case of their concept for one branching level, attractive in practical applications because of its entirely two-dimensional realization with one inlet and one outlet. We demonstrated that even this limiting case, which has not yet been optimized with respect to its number of branching levels, significantly outperforms a fractal, merely bifurcating design. If space considerations allow it, the network performance can be further improved by allowing an extension in the third dimension as additional degree of freedom. The manifold system can be decoupled from the heat-exchanging parallel microchannels by introducing a second plane for the supply and return system that is vertically connected to the heat-exchanging structure. In this way, the manifold system and the heat exchanging parallel channels can be optimized with respect to their channel height independently if the overall cooler height is given.

Acknowledgements

This work was supported by KTI/CTI under project No. P. 8074.1 NMPP-N. We acknowledge Nicole Bieri, Thomas Brunschwiler, Hugo Rothuizen, and Paul Seidler for their contributions, discussions, and support.

References

[1] I. Sauciuc et al., Air-cooling extension – performance limits for processor cooling applications, in: 19th IEEE SEMI-THERM Symposium, 2003.
[2] D.B. Tuckerman, R.F.W. Pease, Implications of high-performance heat sinking for electron devices, IEEE Trans. Electron Devices 28 (10) (1981) 1230–1231.
[3] K.C. Toh, X.Y. Chen, J.C. Chai, Numerical computation of fluid flow and heat transfer in microchannels, Int. J. Heat Mass Transfer 45 (26) (2002) 5133–5141.
[4] X.Q. Wang, C. Yap, A.S. Mujumdar, Effects of two-dimensional roughness in flow in microchannels, J. Electronic Packaging 127 (3) (2005) 357–361.

[5] A. Bejan, M.R. Errera, Deterministic tree networks for fluid flow: geometry for minimal flow resistance between a volume and one point. Fractals-an interdisciplinary, J Complex Geometry Nat. 5 (4) (1997) 685–695.
[6] Y.P. Chen, P. Cheng, Heat transfer and pressure drop in fractal tree-like microchannel nets, Int. J. Heat Mass Transfer 45 (13) (2002) 2643–2648.
[7] D.V. Pence, Reduced pumping power and wall temperature in microchannel heat sinks with fractal-like branching channel networks, Microscale Thermophys. Engng. 6 (4) (2002) 319–330.
[8] X.Q. Wang, A.S. Mujumdar, C. Yap, Thermal characteristics of tree-shaped microchannel nets for cooling of a rectangular heat sink, Int. J. Thermal Sci. 45 (11) (2006) 1103–1112.
[9] X.Q. Wang, A.S. Mujumdar, C. Yap, Numerical analysis of blockage and optimization of heat transfer performance of fractal-like microchannel nets, J. Electronic Packaging 128 (1) (2006) 38–45.
[10] S.T. Liu, Y.C. Zhang, P. Liu, Heat transfer and pressure drop in fractal microchannel heat sink for cooling of electronic chips, Heat Mass Transfer 44 (2) (2007) 221–227.
[11] S.M. Senn, D. Poulikakos, Laminar mixing, heat transfer and pressure drop in tree-like microchannel nets and their application for thermal management in polymer electrolyte fuel cells, J. Power Sources 130 (1–2) (2004) 178–191.
[12] M.M. Yovanovich, Y.S. Muzychka, Solutions of Poisson Equation within Singly and Doubly Connected Prismatic Domains in National Heat Transfer Conference. 1997, AIAA Paper 97-3880: Baltimore, MD.
[13] C.D. Murray, The physiological principle of minimum work: I. The vascular system and the cost of blood volume, Proc. Natl. Acad. Sci. USA 12 (1926) 207–214.
[14] D.B. Tuckerman, R.F.W. Pease, High-performance heat sinking for Vlsi, Electron Device Lett. 2 (5) (1981) 126–129.
[15] Y.S. Muzychka, M.M. Yovanovich, Modeling friction factors in non-circular ducts for developing laminar flow, in: 2nd AIAA Theoretical Fluid Mechanics Meeting. 1998, AIAA Paper 98-2492: Albuquerque, NM.
[16] W. Bohl, in: Technische Stroemungslehre, Vogel, Wuerzburg, 2002, pp. 207–208.
[17] Y.S. Muzychka, M.M. Yovanovich, Laminar forced convection heat transfer in the combined entry region of non-circular ducts, J. Heat Transfer Trans. Asme 126 (1) (2004) 54–61.
[18] E.G. Colgan et al., A practical implementation of silicon microchannel coolers for high power chips, IEEE Trans. Comp. Packaging Technol. 30 (2) (2007) 218–225.
[19] A. Bejan, M.R. Errera, Convective trees of fluid channels for volumetric cooling, Int. J. Heat Mass Transfer 43 (17) (2000) 3105–3118.